COMPONENTS BEAT PATCHES: EIGENVECTOR MASKING FOR VISUAL REPRESENTATION LEARNING

Alice Bizeul[1], **Thomas M. Sutter**[1], **Alain Ryser**[1],
Bernhard Schölkopf[2], **Julius von Kügelgen**[3], **Julia E. Vogt**[1]

`{alice.bizeul,thomas.sutter,alain.ryser,julia.vogt}@inf.ethz.ch`
`bs@tuebingen.mpg.de, julius.vonkuegelgen@math.ethz.ch`

ABSTRACT

Masked Image Modeling has gained prominence as a powerful self-supervised learning approach for visual representation learning by reconstructing masked-out patches of pixels. However, the use of random spatial masking can lead to failure cases in which the learned features are not predictive of downstream labels. In this work, we introduce a novel masking strategy that targets principal components instead of image patches. The learning task then amounts to reconstructing the information of masked-out principal components. The principal components of a dataset contain more global information than patches of pixels, such that the information shared between the masked input and the reconstruction target should involve more high-level variables of interest. This property allows principal components to offer a more meaningful masking space, which manifests in improved quality of the learned representations. We provide empirical evidence across natural and medical datasets and demonstrate substantial improvements in image classification tasks. Our method thus constitutes a simple and robust data-driven alternative to traditional Masked Image Modelling approaches[†]

1 INTRODUCTION

Masked Image Modeling (MIM; Pathak et al., 2016; He et al., 2021; Bao et al., 2022; Xie et al., 2022) draws inspiration from masked language modeling (e.g., BERT; Devlin, 2018), where parts of a sentence are masked, and a model has to learn to predict the missing words. Similarly, in MIM, portions of an image are masked out, and a model has to reconstruct the missing parts from the visible ones. To do well at this task, it is thought that the model is forced to learn a meaningful representation of the visual content in the process (Kong et al., 2023). Empirically, this approach indeed tends to produce representations that perform particularly well when fine-tuned on various downstream tasks, such as image classification and semantic segmentation (He et al., 2021).

The MIM paradigm has led to significant advances in the field of self-supervised learning (SSL) of visual representations (Pathak et al., 2016; Zhou et al., 2021; He et al., 2021; Bao et al., 2022; Xie et al., 2022; Baevski et al., 2022; Dong et al., 2023) and has been particularly effective when combined with Vision Transformers (ViT; Dosovitskiy et al., 2021). A prominent example of this is the Masked Autoencoder (MAE; He et al., 2021), which consists of two core components: a ViT encoder-decoder architecture and a masking strategy that randomly selects a fixed ratio of square image patches. The encoder processes the visible patches (along with their positional embeddings) into a representation that the decoder can use to accurately reconstruct the masked-out content.

While the inner workings of MIM in general, and MAEs in particular, remain under-explored and poorly understood (Zhang et al., 2022; Yue et al., 2023), Kong et al. (2023) recently suggested a potential explanation from a latent variable model perspective: by splitting an image into two parts and asking the model to predict one from the other, MAEs are compelled to pick up on any

---

[†]We release the code to reproduce our results at `https://github.com/alicebizeul/pmae`.
[1] Department of Computer Science, ETH Zürich [2] MPI for Intelligent Systems, Tübingen [3] Seminar for Statistics, ETH Zürich;
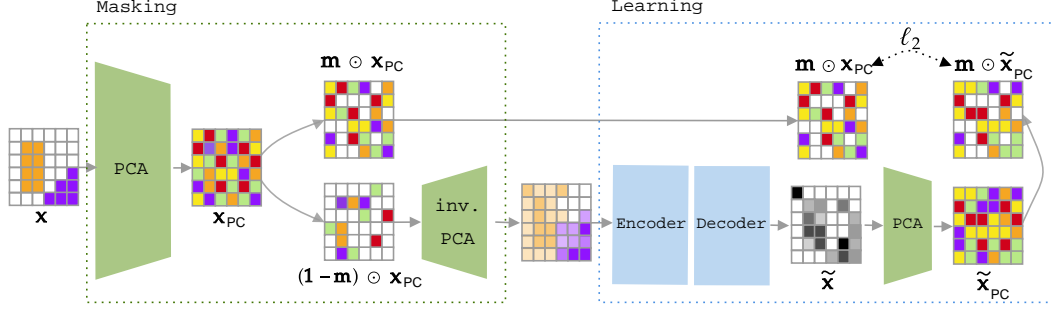
Figure 1: **Overview of the Principal Masked Autoencoder.** A Principal Masked Autoencoder (PMAE) differs from a vanilla MAE by performing the masking in the space of principal components $\mathbf{x}_{PC} = \mathrm{PCA}(\mathbf{x})$ rather than in the observation space. The visible principal components $(\mathbf{1}-\mathbf{m}) \odot \mathbf{x}_{PC}$ are then projected back into the observation space and serve as the input for an encoder-decoder architecture. Masked principal components, $\mathbf{m} \odot \mathbf{x}_{PC}$, serve as the reconstruction target.

information shared between the two that is helpful to solve the image modeling task. If the partition into parts (i.e., the masking strategy) is chosen *carefully*, this shared information will include high-level latent variables, such as object class. Since solving common downstream tasks with a simple (e.g., linear) predictor precisely requires identifying such high-level information, this offers a possible explanation for the observed effectiveness of MIM/MAE representations.

With this in mind, it seems reasonable to ask: *Is patch-wise masking in pixel space really the best strategy for MIM?* In natural language, each word in a sentence tends to carry semantic information, and the information shared between sets of words often conveys the general message of the sentence. However, this does not necessarily apply to the visual domain. In images, individual pixels (and sometimes even entire patches) may contain information redundant that of other pixels. For example, many background pixels will often be identical. Moreover, objects can be masked out completely, such that any information about them is lost and reconstruction becomes impossible (see, e.g., Fig. 2, left). The widely adopted strategy of masking image patches (i.e., *spatial masking*) may thus be sub-optimal and lead to representations that capture information that is irrelevant for downstream tasks of interest.

Some works have thus sought to devise better masking strategies by relying on auxiliary information such as (learned or inferred) image segmentations (Li et al., 2021; Kakogeorgiou et al., 2022; Shi et al., 2022). Without prior knowledge or more complex training pipelines to identify the structure of an image, randomly masking a fixed proportion of patches remains the default practice. However, relying on this strategy assumes—rather unrealistically—that the information shared between any random partition of patches naturally aligns with high-level variables of interest (Kong et al., 2023).

In this work, we introduce *a new data-driven masking strategy for MIM*. Rather than working directly in pixel space, we propose to first project images into a latent space and then perform the masking on the transformed data. Specifically, we opt for off-the-shelf data projections using principal component analysis (PCA) and mask a random subset of the principal components. In PCA, each principal component captures a known percentage of the data's variance, a feature that can inform the masking. We thus propose to mask a set of principal components that carries a *fixed* percentage of the variance, an approach that allows a greater control over the difficulty of the modelling task. We refer to the resulting method as Principal Masked Autoencoder (PMAE), see Fig. 1 for an overview.

We argue that the space of principal components constitutes a more meaningful domain for masking, since it allows for partitioning the information in an image based on global features rather than local patches of pixels. This helps overcome some of the aforementioned failure modes of spatial masking and results in learning more useful high-level representations. Indeed, by masking globally rather than locally, we avoid scenarios where the masked out and visible information are either too strongly correlated (where visible information is redundant with what is masked out) or too weakly correlated (where visible information fails to predict what is masked out). Recent work has also highlighted the beneficial partitioning of image information by PCA: Balestriero & LeCun (2024) demonstrate that low-eigenvalue components capture features crucial for common

Figure 2: **(Left) Masking in pixel space.** TinyImageNet sample (left) with a random spatial mask *partially* removing relevant information (middle) and a random spatial mask removing *all* semantic information (right). The latter constitutes an example in which MIM would likely fail to learn useful representations. **(Right) MedMNIST datasets .** Example images from the (from left to right) DermaMNIST, PathMNIST, and BloodMNIST datasets used for image classification (Yang et al., 2023).

downstream tasks (see also Fig. 7); and Chen et al. (2024b) highlight the importance of the space in which image distortions are applied, referring to PCA as a valuable transformation to consider. To the best of our knowledge, our work is the first to leverage such insights to devise a simple, robust, and effective data-driven alternative to pixel-space-masking in MIM.

We evaluate PMAE in experiments on natural and medical image datasets where it consistently yields substantial performance gains over spatial masking. For linear probing experiments, we report an average performance gain of 38% over the widely adopted strategy of masking out 75% of images patches. Interestingly, we find that without any hyperparameter tuning, PMAE outperforms spatial masking with optimal hyperparameters in all but one dataset. These results support the belief that modeling masked-out principal components facilitates the learning of meaningful representations.

2 BACKGROUND

Principal Component Analysis. Principal Component Analysis (PCA; Pearson, 1901; Hotelling, 1933) identifies components in data that exhibit the highest variance. Given a centered data matrix $\mathbf{X} \in \mathbb{R}^{N \times D}$ with N observations of dimension D, PCA seeks weight vectors $\mathbf{v}_l \in \mathbb{R}^D$ for $l = 1, \ldots, L \leq D$ (principal components, PCs) that maximize the variance of the projections $\mathbf{X}\mathbf{v}_l$, subject to orthogonality with previously found PCs and unit-length constraints. The solution to this problem is given by the eigenvalue decomposition of the empirical covariance matrix $\mathbf{\Sigma} = \mathbf{X}^\top \mathbf{X}$, i.e., $\mathbf{\Sigma} = \mathbf{V}\mathbf{\Lambda}\mathbf{V}^\top$, where $\mathbf{\Lambda} = \text{diag}(\lambda_1, \ldots, \lambda_D)$ contains the eigenvalues $\lambda_1 > \ldots > \lambda_D$, and $\mathbf{V} \in \mathbb{R}^{D \times D}$ contains the corresponding eigenvectors. The first L PCs correspond to the eigenvectors of $\mathbf{\Sigma}$ with the largest eigenvalues, capturing the dominant modes of variation in the data, with each PC's explained variance proportional to its eigenvalue λ_l. While PCA is often used with $L < D$ for dimensionality reduction, we focus on the lossless case where $L = D$. The projection of $\mathbf{X}$ onto its principal components (*"into PC space"*) is given by $\mathbf{X}_{\text{PC}} = \mathbf{X}\mathbf{V}$, with the inverse transformation $\mathbf{X} = \mathbf{X}_{\text{PC}}\mathbf{V}^\top$. Since $\mathbf{V}$ is an orthonormal basis, the independence of $\mathbf{X}_{\text{PC}}$'s columns depends on the structure of $\mathbf{X}$. If $\mathbf{X}$'s columns are linear combinations of independent factors, $\mathbf{X}_{\text{PC}}$'s columns *may* be independent. However, if $\mathbf{X}$'s columns are non-linear combinations of independent factors, $\mathbf{X}_{\text{PC}}$'s columns *cannot* be independent. Our work focuses on natural images, a domain in which pixel values are widely regarded as the result of a *non-linear* generative process. Please refer to Appx. A.1 for more details regarding PCA.

Representation Learning. Representation learning (Bengio et al., 2013) aims at learning an embedding function $f : \mathbf{x} \mapsto \mathbf{z}$, which maps data observation $\mathbf{x} \in \mathbb{R}^D$ to latent representation $\mathbf{z} \in \mathbb{R}^K$. These latent representations are meant to capture some of the explanatory factors underlying the data, thus making $\mathbf{z}$ well-suited for use in downstream tasks such as predicting y (e.g., the class or location of objects), often thought of as a being a function of the data's explanatory variables.

Masked Image Modelling. Prominent approaches to representation learning in the image domain rely on the masked image modeling paradigm (Pathak et al., 2016; Zhou et al., 2021; He et al., 2021; Bao et al., 2022). We choose the widely adopted Masked Autoencoder (He et al., 2021) as a representative of MIM. The encoder-decoder architecture in MAE allows the model to reconstruct
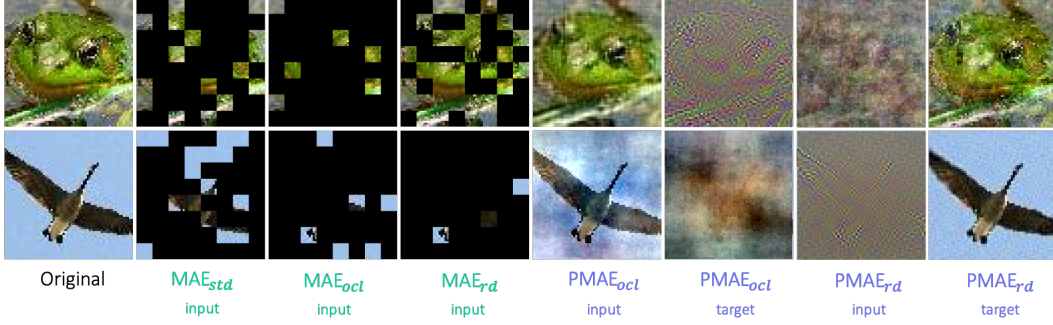
Figure 3: **Mask Design Strategies.** An overview of the different mask design strategies used in our experimental setup: spatial masking (*green*) and principal component masking (*blue*). *std* refers to the standard approach of masking out 75% of image patches, *ocl* denotes masking with the optimal masking ratio, *rd* represents a randomized strategy where the masking ratio is randomly sampled for each batch, and *target* refers to the reconstruction target;

masked portions of data observations by leveraging the learned latent representations:

$$\mathcal{L}_{\text{MAE}}(\mathbf{x}, \mathbf{m}; \boldsymbol{\theta}, \boldsymbol{\phi}) = \|(\mathbf{1} - \mathbf{m}) \odot g_{\boldsymbol{\theta}}(f_{\boldsymbol{\phi}}(\mathbf{m} \odot \mathbf{x})) - (\mathbf{1} - \mathbf{m}) \odot \mathbf{x}\|_2^2, \quad (2.1)$$

where $\mathbf{x}$ is a data observation and $\mathbf{m}$ and $(\mathbf{1} - \mathbf{m})$ are complementary binary masks used to extract the visible and masked-out parts of the data, respectively. $\odot$ is the element-wise product operation. The embedding function f, parametrized by $\boldsymbol{\phi}$, encodes the visible portions of the input together with their positional embeddings, while the decoder function g, parametrized by $\boldsymbol{\theta}$, reconstructs the missing parts from their positional embeddings and the latent representation $\boldsymbol{z} = f_{\boldsymbol{\phi}}(\mathbf{m} \odot \mathbf{x})$.

The binary mask $\mathbf{m} = \{m^i\}_{i=1}^D$ partitions the D pixels into two disjoint sets of $(1 - r)D$ visible and rD masked out pixels, where r is referred to as the *masking ratio*. Patch-wise masking, which masks patches of pixels instead of individual pixels, introduces the patch size as an additional hyperparameter. r then defines the amount of patches to be masked out. Prior work has relied on hyperparameter sweeps to identify the masking ratio and patch size that optimize downstream performance (He et al., 2021; Zhang et al., 2022). These efforts have led to the widely adopted approach of masking out 75%—$r = 0.75$—of image patches.

Intuition behind MIM. Despite the MIM paradigm with random spatial masking producing strong results on representation learning benchmarks (Dong et al., 2023), it is based on the rather unrealistic assumption that for any partition of an image's patches into two disjoint sets, the information shared by these sets contains y (Kong et al., 2023). In Fig. 2, we observe that while some masks (middle image) may allow shared information to include the object type and corresponding class label, there are many partitions where predicting the label (e.g., the class label *"goose"* in Fig. 2) from the visible patches is almost as uncertain as a random guess (left image). Moreover, even for well-designed masks, a substantial proportion of masked-out patches contain information redundant with visible pixels. We conjecture that, as a result, Masked Image Modeling with spatial masking leads to a suboptimal learning approach that is misaligned with common downstream tasks, is characterized by slow convergence and suffers from high sensitivity to hyperparameters, as suggested by prior work (He et al., 2021; Balestriero & LeCun, 2024) and confirmed in Section 5.

3 ROBUST MASKED IMAGE MODELLING

To address the challenges presented in Section 2, we propose *Principal Masked Autoencoders* (PMAE). PMAE builds on the MIM learning paradigm, but differs from prior approaches by performing the masking operation in a learned latent space, resulting in the following objective:

$$\mathcal{L}_{\text{PMAE}}(\mathbf{x}, \mathbf{m}; \boldsymbol{\theta}, \boldsymbol{\phi}) = \|(\mathbf{1} - \mathbf{m}) \odot t(g_{\boldsymbol{\theta}}(f_{\boldsymbol{\phi}}(t^{-1}(\mathbf{m} \odot t(\mathbf{x}))))) - (\mathbf{1} - \mathbf{m}) \odot t(\mathbf{x})\|_2^2, \quad (3.1)$$

where t is an invertible function, $t : \mathbb{R}^D \to \mathbb{R}^D$, mapping the input $\mathbf{x}$ to a representation space. Eq. (3.1) differ from Eq. (2.1) in that the masking operates within the latent space, $t(\boldsymbol{x})$. Similar

4

to Eq. (2.1), the embedding function f, parametrized by ϕ, encodes the visible portions of the input together with their positional embeddings, while the decoder function g, parametrized by θ, reconstructs the missing parts. Note that Eq. (2.1) is a special case of Eq. (3.1) where t is the identity mapping. Fig. 1 provides a visual summary of PMAE for when t is the PCA.

Design Choices in PMAE. While Eq. (3.1) is general enough to accommodate any invertible mapping t, this work specifically explores the Principal Component Analysis (PCA) as t, where $\mathbf{x}_{PC} = t(\mathbf{x})$, leaving the investigation of alternative image transformations (e.g., Fourier transform) to future work. We further discuss extensions to other latent spaces in Section 8.

Following MAEs, we use Vision Transformers (ViT; Dosovitskiy et al., 2021) for both f and g. Since these architectures are optimized for processing images, we maintain the encoding and decoding operations in the space of observations. After masking in latent space, t^{-1} maps $\mathbf{x}_{PC}$ back to the pixel space. Masked Image Modeling (MIM) frameworks are often coupled with ViTs, likely due to the use of binary masks in pixel space. These masks produce images with black-patch occlusions (as shown in Fig. 3), which appear poorly aligned with the inductive biases of other architectures, such as convolutional networks. Instead, PMAE seem compatible with convolutional networks. By masking principal components rather than patches of pixels, the inputs to the encoder in PMAE display smoother patterns of activation (see Fig. 3). The exploration of other architectural choices for PMAE is left for future work.

We construct Eq. (3.1) to closely align with the MAE setup, focusing solely on penalizing reconstruction errors on masked-out information. Eq. (3.1) minimizes the reconstruction error in the principal component space. In Eq. (A.1), presented in Appx. A.7.3, we also investigated an alternative approach where the error is minimized in the space of observations: the decoder's output is kept as is and the masked-out principal components are projected back to pixel space. However, this alternative results in lower downstream performance, possibly due to the stricter constraints imposed on the decoder's output, motivating our focus on Eq. (3.1).

The design of the masks also represents an important design choice. In MAEs, a fixed percentage of pixels is masked out without any further considerations about the underlying data structure. PMAE, on the other hand, employs a more data-driven strategy by utilizing information about the variance captured by each principal component to guide the mask design. In PCA, the variance explained by a principal component is proportional to its eigenvalue. Leveraging this relationship, we systematically mask components that collectively account for a fixed percentage of the dataset's variance. Fig. 4 illustrates this process. After applying PCA, the order of the principal components is randomly shuffled for each batch. The components are then divided into two disjoint sets: one explaining $100 \times (1-r)\%$ of the variance and the other $100 \times r\%$, with r corresponding to the masking ratio. Details on the choice of r are provided in Section 4.
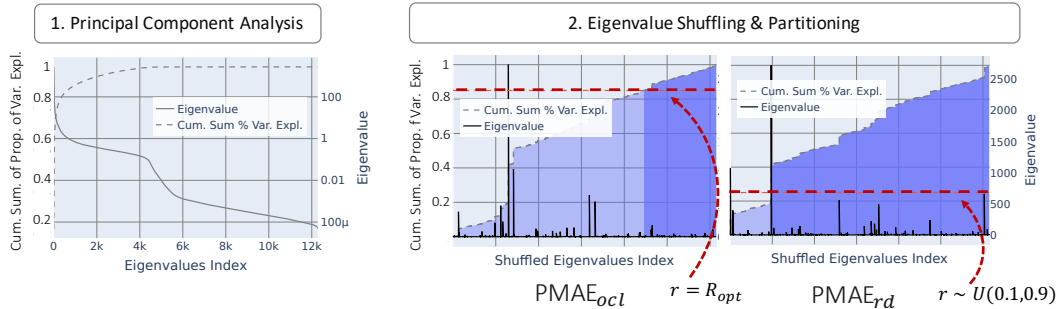

Figure 4: **Mask Design in PMAE.** 1. Perform Principal Component Analysis 2. For each batch, randomly shuffle the principal components and select a subset to construct the input (light blue), while the remaining components are used to create the reconstruction target (dark blue). In PMAE$_{ocl}$, the input components are chosen to explain $100 \times (1-r)\%$ of the data's variance with r optimized for downstream performance (here $R_{opt} = 0.15$). In PMAE$_{rd}$, the input explains between 10% and 90% of the variance with r sampled independently and uniformly in $[10, 90]$ for each batch.

Intuition behind PMAE. In contrast to the traditional spatial masking presented in Section 2, an appropriate function t can encourage information shared between visible and masked-out information to contain y. More specifically, if the latent space captures unique global information in each dimension, masking any of these dimensions retains information about all parts of the image. Hence, Eq. (A.1) allows us to learn more meaningful representations for a suitable choice of t. While there may be many appropriate choices for t, we found that applying PCA and projecting samples using the resulting principal components is a suitable choice for the latent space. In particular, each dimension captures specific factors of variation observed within the dataset and is typically tied to global features as shown in Fig. 7. Masking one factor of variation thus prevents us from completely removing all information about variables of interest within a sample, as most principal components will retain some information about them.

In PMAE, the masking ratio—the proportion of explained variance masked—can also easily be interpreted, as it directly corresponds to a well-understood quantity. In contrast, masking patches of pixels lacks such a straightforward connection to a well-defined metric. Depending on the dataset, a given proportion of masked patches can correspond to varying amounts of information content, making the masking ratio in the spatial domain harder to interpret.

We will present the positive impact of this reasoning in Section 5, where we compare principal component and observation space masking empirically. In Section 6, we will provide additional intuition as to why PCA leads to a suitable masking strategy.

4 EXPERIMENTAL SETUP

We now outline the setup used to validate PMAE. Our experiments adapt the implementation proposed by He et al. (2021), ensuring the comparability of results between our PMAE and the MAE baseline. Further experimental details and computational costs can be found in Appx. A.2.

Mask Design. State-of-the-art MIM models, like MAE (He et al., 2021), typically employ random image patch masking, which serves as our baseline. Based on ablation studies from He et al. (2021), the standard practice involves masking out 75% of image patches (denoted as MAE_{std}). We also examine an oracle-based masking strategy (denoted as MAE_{ocl}), where the masking ratio is fine-tuned to optimize linear probing downstream performance. This setting serves as an upper-bound to the downstream performance. Additionally, we introduce a randomized masking approach, MAE_{rd}, in which the masking ratio is independently sampled for each batch, within a range of 10% to 90% of image patches being masked out. This strategy is exempt from any hyperparameter tuning and offers insights into the downstream performance when using suboptimal masking hyperparameters.

A similar approach is applied to PMAE, where we consider both oracle (PMAE_{ocl}) and randomized (PMAE_{rd}) masking strategies. In the oracle approach, we define the optimal percentage of *variance* to be masked based on linear probe downstream performance on a held-out dataset. In the randomized strategy, we simply ensure at least 10% and at most 90% of the data variance is masked out. This percentage is independently sampled for each batch.

Fig. 3 provides examples of the images obtained from these masking strategies. Note that Fig. 3 helps visualise how MAE masks out patches of local information while PMAE operates globally over the image.

Training & Evaluation. We train ViT-T/8 encoder and decoder backbones (Dosovitskiy et al., 2021). Following He et al. (2021), we use image flipping and random image cropping as data augmentations. The decoder's output is normalized (He et al., 2021) for MAEs only as this did not result in a consistent performance gain for PMAEs. We train representations for 800 epochs and provide an overview of the evolution of performance across training in Appx. A.7. We then evaluate learned representations on image classification using a linear probe and multi-layer perceptron (MLP) classifier on top of the encoder's output `[CLS]` token which is frozen. Additionally, we also explore the fine-tuning setting in which the pre-trained encoder and a linear probe appended to the `[CLS]` token are trained simultaneously. Following He et al. (2021), we fix the training duration at evaluation to 100 epochs. Appx. A.7 also reports downstream performance obtained with a k-NN classifier.
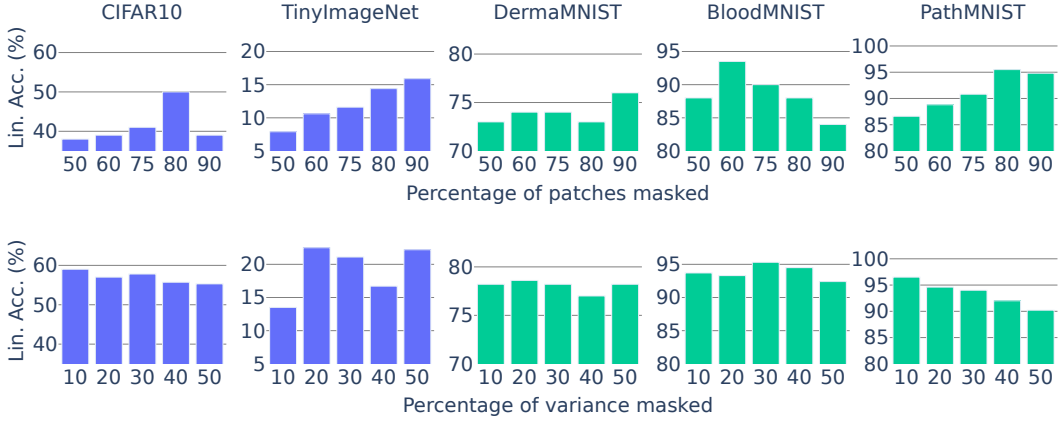
Figure 5: **Impact of the Masking Ratio.** MAE (top) and PMAE (bottom) linear probing accuracy for varying masking ratios. The masking ratio is a sensitive and data-dependent hyper-parameter. While for MAE a clear masking guideline is hard to extract, for PMAE we observe a close to optimal performance across datasets for 20% of the data variance masked.

5 RESULTS

In this section, we will outline and analyze the empirical advantages of PMAE compared to standard MAEs in image classification tasks. Specifically, we provide evidence that masking within the space of principal components facilitates the learning of discriminative features, resulting in improved performance on downstream tasks. Our findings are supported by empirical evidence across diverse datasets, including two natural image datasets of 32×32 and 64×64 resolutions, and three medical datasets taken from MedMNIST (Yang et al., 2023) of 64×64 resolution (see Fig. 2 for example MedMNIST images).

Tab. 1 presents the classification accuracy using both a linear probe and a MLP classifier. Across datasets, we observe substantial improvements with $PMAE_{ocl}$ in linear probing compared to the standard MAE_{std}, with an average increase of 38% ($+14$ percentage points). Additionally, $PMAE_{ocl}$ outperforms MAE_{ocl} by 20.3% ($+9.5$ percentage points). We see similar gains with the randomized hyperparameter strategy. PMAE consistently outperforms MAE across all datasets, yielding an average performance increase of 29.9% ($+5.4$ percentage points), even when sub-optimal hyperparameters are used. These findings also extend to the non-linear evaluation setting, (see the middle part of Tab. 1). The bottom part of Tab. 1 presents the downstream performance in the fine-tuning setting. We continue to observe a performance gain brought by PMAE over MAE of 2.3% ($+8.8$ percentage points) on average. For two of the MedMNIST datasets we observe an equal and high ($>98\%$) performance for both methods, showcasing that these tasks are easily completed by both approaches.

These empirical findings lead to several conclusions. First, we observe that the recommended masking of 75% of image patches is largely sub-optimal *across* datasets. Figs. 5 and 11 report an ablation study of the masking ratios for MAE and PMAE. Fig. 5 (top) shows that, across all five datasets, a 75% masking ratio is sub-optimal. For PMAE, the masking ratio seems to be a more stable hyperparameter. Fig. 5 (bottom) shows that across all evaluated datasets we observe the best or near-optimal performance for PMAE at 20% of the variance masked. Second, we validate the empirical benefits brought by PMAE. Interestingly, we notice that PMAE without any hyperparameter tuning ($PMAE_{rd}$) outperforms MAE with optimum masking ratio in all but one case (i.e., CIFAR10). Finally, investing in hyperparameter tuning for PMAE leads to substantial performance gains over MAE.

Fig. 6 provides a deeper look into downstream performance across different training epochs and the variability of results with varying masking ratios. As shown in Fig. 6 (left), the advantages of PMAE become evident after just a hundred training epochs. Notably, training PMAE for 100 epochs exceeds the performance of MAE after 800 epochs. Additional figures for other datasets can be found in Appx. A.7. Furthermore, Fig. 6 (right) explores how downstream accuracy fluctuates with

different masking ratios. Our analysis reveals that PMAE displays comparable or lower standard errors across these conditions in contrast to MAE. Collectively, these results suggest that PMAE's masking strategy enhances the alignment between image reconstruction and image classification tasks more effectively than the MAE objective.

Table 1: Linear & MLP probe and fine-tuning top-1% accuracy for CIFAR10, TinyImageNet and MedMNIST datasets for random masking in pixel (MAE) and principal component (PMAE) space with the standard 75% (std), oracle (ocl) and random (rd) masking ratios. * refers to ours.

		CIFAR10	TinyImageNet	DermaMNIST	BloodMNIST	PathMNIST
Linear	MAE_{std}	41.7	11.5	72.4	73.4	83.4
	MAE_{ocl}	50.7	15.5	73.7	78.6	86.4
	$PMAE^\star_{ocl}$	**59.0**	**22.5**	**78.6**	**95.5**	**96.8**
	MAE_{rd}	41.9	7.5	72.4	83.2	85.6
	$PMAE^\star_{rd}$	**44.0**	**16.9**	**76.4**	**90.0**	**90.1**
MLP	MAE_{std}	34.0	15.5	72.2	68.6	92.6
	MAE_{ocl}	55.2	22.2	74.4	75.8	95.1
	$PMAE^\star_{ocl}$	**64.1**	**25.1**	**80.2**	**92.5**	**98.6**
	MAE_{rd}	38.5	11.6	66.9	70.6	95.7
	$PMAE^\star_{rd}$	**47.0**	**22.6**	**77.4**	**80.2**	**97.7**
Fine-tuned	MAE_{std}	75.7	37.5	80.4	97.8	**99.7**
	MAE_{ocl}	80.5	42.8	79.9	**98.1**	**99.7**
	$PMAE^\star_{ocl}$	**84.8**	**44.5**	**82.3**	**98.1**	**99.7**
	MAE_{rd}	77.3	39.7	79.6	97.4	99.6
	$PMAE^\star_{rd}$	**80.4**	**46.9**	**82.4**	**98.5**	**99.7**

6 UNDERSTANDING PMAE

In this section, we aim to provide more intuition as to why masking *components* rather than *image patches* leads to more robust objectives. In Section 2, we discuss the hypothesis under which MIM operates (Kong et al., 2023) and present an example failure case of spatial masking in Fig. 2. We highlight how masking pixels can lead to a misalignment between the MIM objective and the learning of meaningful representations. If all patches covering an object are masked out, it is uncertain whether the remaining patches share any information with the object. Contrary, if the masked out information is redundant with the information carried by visible patches, it is likely that the information shared does not contain the object class but rather perceptual features (e.g., colors or textures).
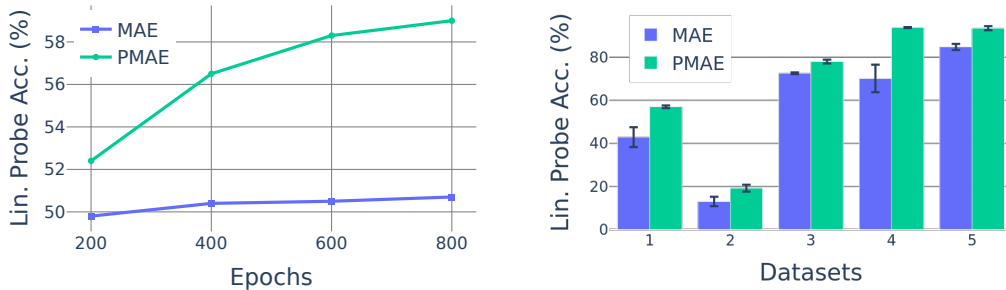

Figure 6: **(Left) Learning curves.** Linear probe accuracy for CIFAR10 classification across the number of training epochs. PMAE outperforms MAE's final performance even after short training times. **(Right) Ablation study of the masking ratio.** Average and standard error of the linear probe accuracy across masking ratios for MAE and PMAE. We observe lower or equivalent standard errors for PMAE than for MAE across CIFAR10 (1), TinyImageNet (2) and MedMNIST (3-5) datasets.

Different from spatial masking, masking principal *components* leads to the removal of global image features, instead of only acting locally as in spatial masking. Fig. 7 serves as an example highlighting the correspondence between principal component and perceptual features. In this example, the principal components with the highest eigenvalues capture the colors within the image while the bottom PCs highlight the edges. Early work in image processing (Turk & Pentland, 1991) has demonstrated this connection between an image's dominant modes of variation and its low spatial frequency components, providing further intuition for how information is partitioned in the space of PCs of natural images.

By removing a subset of principal components, PMAE prevents the removal of all the information characterizing an object and prevents redundant information to remain after masking. Instead, PMAE drops a set of unique image components. By taking advantage of the information partitioning in PCA, PMAE thereby mitigates MAE's failure cases, ultimately leading to increased accuracy. Although the potential of the principal component space for Masked Image Modelling (Balestriero & LeCun, 2024) or Image Denoising (Chen et al., 2024b) has been recently explored, our work is the first to propose an effective masking strategy that directly leverages PCA.

7 RELATED WORK

Self-supervised learning. Self-supervised learning (SSL) leverages auxiliary tasks to learn from unlabeled data, often outperforming supervised methods on downstream tasks. SSL can be divided into two categories: discriminative and generative (Liu et al., 2021). Discriminative methods (Chen et al., 2020a; Caron et al., 2021) focus on enforcing invariance or equivariance between data views in the representation space, while generative methods (He et al., 2021; Bizeul et al., 2024) rely on data reconstruction from, often, corrupted observations. Though generative methods historically lagged in performance, recent work has bridged the gap by integrating strengths from both paradigms (Assran et al., 2022; Dong et al., 2023; Oquab et al., 2023; Chen et al., 2024a; Lehner et al., 2023). Interestingly, recent discriminative methods employ multi-cropping strategies to create distinct data views (Oquab et al., 2023; Assran et al., 2023), which is reminiscent of image masking. Balestriero & LeCun (2024) point out the misalignment between auxiliary and downstream tasks in reconstruction-based SSL and suggest novel masking strategies to help realign these objectives.

Masked Image Modelling. MIM extends the successful masked language modeling paradigm to vision tasks. Early methods, such as Context Encoder (Pathak et al., 2016), used a convolutional autoencoder to inpaint a central region of the image. The rise of Vision Transformers (ViTs) (Dosovitskiy et al., 2021) has driven significant advancements in MIM. BEiT (Zhou et al., 2021; Bao et al., 2022) combines a ViT encoder with image tokenizers (Ramesh et al., 2021) to predict discrete tokens for masked patches. SimMIM (Xie et al., 2022) simplifies the task by pairing a ViT encoder with a regression head to directly predict raw pixel values for the masked regions. MAE (He et al., 2021) introduces a more efficient encoder-decoder architecture, with a shallow decoder. MIM's domain-agnostic masking strategies have also proven effective in multi-modal tasks (Baevski et al., 2022; Bachmann et al., 2022).

Mask Design Strategies. A critical component of the Masked Image Modeling paradigm is the design of effective masking strategies. Early MIM approaches have relied on random spatial masking techniques, such as masking out the central region of an image (Pathak et al., 2016), image patches (He et al., 2021; Xie et al., 2022), and blocks of patches (Bao et al., 2022). Inspired by advances in language modeling, recent efforts have explored semantically guided mask design. Li et al. (2021) use self-attention maps to mask irrelevant regions, while Kakogeorgiou et al. (2022) focus on masking semantically rich areas. Shi et al. (2022) design masks through adversarial learning, where the resulting masks resemble semantic maps, a concept extended by Li et al. (2022a) through progressive semantic region masking. Further advancing this direction, Wang et al. (2023) and Madan et al. (2024) introduce curriculum learning-inspired mask design methods. These methods often require additional training steps, components, or more complex objectives. More closely related to our work, Chang et al. (2022); Chen et al. (2024b) explore the use of pre-existing image representations for asked Image Modeling and image denoising. Chen et al. (2024b) introduce additive Gaussian noise to principal components as an alternative to the traditional Denoising Autoencoders. Chang
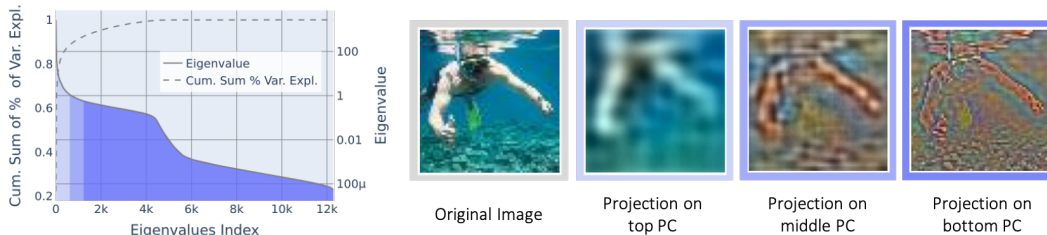
Figure 7: **From Principal Components to Spatial Features.** Overview of the spatial features associated with distinct regions of the principal component (PC) spectrum; Images depict the features encapsulated by the top PCs (light blue), middle PCs (mild blue) and bottom PCs (dark blue).

et al. (2022) utilize masked token modeling by leveraging the discrete latent space of a pre-trained VQVAE to develop an image generation model.

8 DISCUSSION

In this work, we have investigated different masking strategies for Masked Image Modelling (MIM). To this end, we have introduced the Principal Masked Autoencoder (PMAE) as an alternative to masking random patches of pixels. PMAE is rooted in Principal Component Analysis (PCA; Pearson, 1901; Hotelling, 1933), which is a widely used data-driven *linear* transformation. Unlike recent alternatives that require additional supervision, learnable components, or complex training pipelines (Li et al., 2021; 2022a; Kakogeorgiou et al., 2022; Li et al., 2022b), PMAE stays close to the core principles of MIM: the combination of a randomized masking strategy and an encoder-decoder architecture. Despite its simplicity, we demonstrate that PMAE yields substantial performance improvements over spatial masking on image classification tasks. Further, in a PMAE, the masking ratio—typically a sensitive and difficult-to-tune hyperparameter in MIM—appears more robust and has a natural interpretation as the ratio of variance explained by the masked input.

Since PCA is easily applicable to any data modality, our proposal of masking principal components is not specific to MIM. Instead, it can be viewed as a *general strategy* that should also be applicable to other types of modalities beyond images, as well as to other self-supervised learning (SSL) approaches. Indeed, data masking is commonly adopted in discriminative SSL methods. Whereas early approaches, such as SimCLR (Chen et al., 2020a) or MoCo (Chen et al., 2020b), relied on combinations of image transformations (e.g., color jitter, flips, crops, etc.) as data augmentation strategies, more recent state-of-the-art methods like DINO (Caron et al., 2021; Oquab et al., 2023) and I-JEPA (Assran et al., 2023) have shifted to relying solely on image cropping, which can be considered a type of masking. The integration of principal component masking instead of image cropping into such SSL pipelines constitutes a promising future direction of research.

In the present work, we have focused on PCA as a meaningful masking space. However, our core idea of masking a *transformed* version of the data (rather than the *raw* data) can be viewed as laying the groundwork for other, more generic approaches to information masking in self-supervised representation learning. Moving beyond PCA, a natural extension would be to *learn* a suitable latent space in which the masking is performed. This route has the added potential of leveraging recent theoretical insights (Kong et al., 2023) by more explicitly enforcing that the shared information between visible and masked-out latent components contains high-level latent variables that are most useful for the downstream tasks of interest. Other off-the-shelf *non-linear* transformations, such as the Fourier transform (Bracewell & Kahn, 1966), Wavelet transform (Daubechies, 1992), Kernel Principal Component Analysis (Schölkopf et al., 1997), or Diffusion Maps (Coifman & Lafon, 2006), represent alternative candidate transformations. Future research should explore whether the properties of these spaces provide comparable or additional advantages over PCA. Preliminary results on Kernel PCA, presented in Appx. A.7.5, demonstrate performance gains over PMAE, motivating further exploration. A particularly appealing aspect of some of these methods (e.g., Fourier & Wavelet transforms and Diffusion Maps) is the use of fixed bases, which could eliminate the computational overhead of PCA—whose cost scales cubically with the data dimensionality—and improve scalability to larger datasets.

9 ACKNOWLEDGMENTS

REFERENCES

Mahmoud Assran, Mathilde Caron, Ishan Misra, Piotr Bojanowski, Florian Bordes, Pascal Vincent, Armand Joulin, Michael Rabbat, and Nicolas Ballas. Masked siamese networks for label-efficient learning, 2022. URL http://arxiv.org/abs/2204.07141. [Cited on p. 9.]

Mahmoud Assran, Quentin Duval, Ishan Misra, Piotr Bojanowski, Pascal Vincent, Michael Rabbat, Yann LeCun, and Nicolas Ballas. Self-supervised learning from images with a joint-embedding predictive architecture. pp. 15619–15629, 2023. URL https://openaccess.thecvf.com/content/CVPR2023/html/Assran_ Self-Supervised_Learning_From_Images_With_a_Joint-Embedding_ Predictive_Architecture_CVPR_2023_paper.html. [Cited on p. 9 and 10.]

Roman Bachmann, David Mizrahi, Andrei Atanov, and Amir Zamir. Multimae: Multi-modal multitask masked autoencoders. In *European Conference on Computer Vision*, pp. 348–367. Springer, 2022. URL https://arxiv.org/pdf/2204.01678. [Cited on p. 9.]

Alexei Baevski, Wei-Ning Hsu, Qiantong Xu, Arun Babu, Jiatao Gu, and Michael Auli. data2vec: A general framework for self-supervised learning in speech, vision and language. In *Proceedings of the 39th International Conference on Machine Learning*, pp. 1298–1312. PMLR, 2022. URL https://proceedings.mlr.press/v162/baevski22a.html. ISSN: 2640-3498. [Cited on p. 1 and 9.]

Randall Balestriero and Yann LeCun. Learning by reconstruction produces uninformative features for perception, 2024. URL http://arxiv.org/abs/2402.11337. [Cited on p. 2, 4, and 9.]

Hangbo Bao, Li Dong, Songhao Piao, and Furu Wei. BEiT: BERT pre-training of image transformers, 2022. URL http://arxiv.org/abs/2106.08254. [Cited on p. 1, 3, and 9.]

Yoshua Bengio, Aaron Courville, and Pascal Vincent. Representation learning: A review and new perspectives. *IEEE transactions on pattern analysis and machine intelligence*, 35(8):1798–1828, 2013. URL https://arxiv.org/pdf/1206.5538. [Cited on p. 3.]

Alice Bizeul, Bernhard Schölkopf, and Carl Allen. A probabilistic model to explain self-supervised representation learning. *Transactions on Machine Learning Research*, 2024. URL https://arxiv.org/pdf/2402.01399. [Cited on p. 9.]

Ron Bracewell and Peter B Kahn. The fourier transform and its applications. *American Journal of Physics*, 34(8):712–712, 1966. [Cited on p. 10.]

Mathilde Caron, Hugo Touvron, Ishan Misra, Hervé Jégou, Julien Mairal, Piotr Bojanowski, and Armand Joulin. Emerging properties in self-supervised vision transformers, 2021. URL http://arxiv.org/abs/2104.14294. [Cited on p. 9 and 10.]

Huiwen Chang, Han Zhang, Lu Jiang, Ce Liu, and William T Freeman. Maskgit: Masked generative image transformer. In *Proceedings of the IEEE/CVF Conference on Computer Vision and Pattern Recognition*, pp. 11315–11325, 2022. URL https://openaccess.thecvf.com/content/CVPR2022/papers/Chang_ MaskGIT_Masked_Generative_Image_Transformer_CVPR_2022_paper.pdf. [Cited on p. 9.]

Ting Chen, Simon Kornblith, Mohammad Norouzi, and Geoffrey Hinton. A simple framework for contrastive learning of visual representations. In *International conference on machine learning*, pp. 1597–1607. PMLR, 2020a. URL http://proceedings.mlr.press/v119/ chen20j/chen20j.pdf. [Cited on p. 9 and 10.]

Xiaokang Chen, Mingyu Ding, Xiaodi Wang, Ying Xin, Shentong Mo, Yunhao Wang, Shumin Han, Ping Luo, Gang Zeng, and Jingdong Wang. Context autoencoder for self-supervised representation learning. *International Journal of Computer Vision*, 132(1): 208–223, 2024a. URL https://link.springer.com/content/pdf/10.1007/s11263-023-01852-4.pdf. [Cited on p. 9.]

Xinlei Chen, Haoqi Fan, Ross Girshick, and Kaiming He. Improved baselines with momentum contrastive learning. *arXiv preprint arXiv:2003.04297*, 2020b. URL https://arxiv.org/abs/2003.04297. [Cited on p. 10.]

Xinlei Chen, Zhuang Liu, Saining Xie, and Kaiming He. Deconstructing denoising diffusion models for self-supervised learning. *arXiv preprint arXiv:2401.14404*, 2024b. URL https://arxiv.org/pdf/2401.14404. [Cited on p. 3 and 9.]

Ronald R Coifman and Stéphane Lafon. Diffusion maps. *Applied and computational harmonic analysis*, 21(1):5–30, 2006. URL https://d1wqtxts1xzle7.cloudfront.net/46791646/j.acha.2006.04.00620160625-29758-1cjigj-libre.pdf. [Cited on p. 10.]

Ingrid Daubechies. Ten lectures on wavelets. *Society for industrial and applied mathematics*, 1992. URL https://epubs.siam.org/doi/pdf/10.1137/1.9781611970104.fm. [Cited on p. 10.]

Jacob Devlin. Bert: Pre-training of deep bidirectional transformers for language understanding. *arXiv preprint arXiv:1810.04805*, 2018. URL https://bibbase.org/service/mendeley/bfbbf840-4c42-3914-a463-19024f50b30c/file/6375d223-e085-74b3-392f-f3fed829cd72/Devlin_et_al___2019___BERT_Pre_training_of_Deep_Bidirectional_Transform.pdf.pdf. [Cited on p. 1.]

Xiaoyi Dong, Jianmin Bao, Ting Zhang, Dongdong Chen, Weiming Zhang, Lu Yuan, Dong Chen, Fang Wen, Nenghai Yu, and Baining Guo. Peco: Perceptual codebook for bert pre-training of vision transformers. In *Proceedings of the AAAI Conference on Artificial Intelligence*, volume 37, pp. 552–560, 2023. URL https://arxiv.org/pdf/2111.12710. [Cited on p. 1, 4, and 9.]

Alexey Dosovitskiy, Lucas Beyer, Alexander Kolesnikov, Dirk Weissenborn, Xiaohua Zhai, Thomas Unterthiner, Mostafa Dehghani, Matthias Minderer, Georg Heigold, Sylvain Gelly, Jakob Uszkoreit, and Neil Houlsby. An image is worth 16x16 words: Transformers for image recognition at scale, 2021. URL http://arxiv.org/abs/2010.11929. [Cited on p. 1, 5, 6, and 9.]

P Goyal. Accurate, large minibatch sg d: training imagenet in 1 hour. *arXiv preprint arXiv:1706.02677*, 2017. URL https://scidirect.org/pdf/download/accurate-large-minibatch-sgd-training-imagenet-in-00YnBBGKeCb.pdf. [Cited on p. 16.]

Kaiming He, Xinlei Chen, Saining Xie, Yanghao Li, Piotr Dollár, and Ross Girshick. Masked autoencoders are scalable vision learners, 2021. URL http://arxiv.org/abs/2111.06377. [Cited on p. 1, 3, 4, 6, 9, 15, 16, and 20.]

Harold Hotelling. Analysis of a complex of statistical variables into principal components. *Journal of educational psychology*, 24(6):417, 1933. URL https://www.cis.rit.edu/~rlepci/Erho/Derek/Useful_References/Principal%20Components%20Analysis/Hotelling_PCA_part1.pdf. [Cited on p. 3, 10, and 15.]

Ioannis Kakogeorgiou, Spyros Gidaris, Bill Psomas, Yannis Avrithis, Andrei Bursuc, Konstantinos Karantzalos, and Nikos Komodakis. What to hide from your students: Attention-guided masked image modeling. In Shai Avidan, Gabriel Brostow, Moustapha Cissé, Giovanni Maria Farinella, and Tal Hassner (eds.), *Computer Vision – ECCV 2022*, pp. 300–318. Springer Nature Switzerland, 2022. ISBN 978-3-031-20056-4. doi: 10.1007/978-3-031-20056-4_18. URL https://link.springer.com/chapter/10.1007/978-3-031-20056-4_18. [Cited on p. 2, 9, and 10.]

Lingjing Kong, Martin Q Ma, Guangyi Chen, Eric P Xing, Yuejie Chi, Louis-Philippe Morency, and Kun Zhang. Understanding masked autoencoders via hierarchical latent variable models. In *Proceedings of the IEEE/CVF Conference on Computer Vision and Pattern Recognition*, pp. 7918–7928, 2023. URL https://arxiv.org/abs/2306.04898. [Cited on p. 1, 2, 4, 8, and 10.]

Johannes Lehner, Benedikt Alkin, Andreas Fürst, Elisabeth Rumetshofer, Lukas Miklautz, and Sepp Hochreiter. Contrastive tuning: A little help to make masked autoencoders forget, 2023. URL http://arxiv.org/abs/2304.10520. [Cited on p. 9.]

Gang Li, Heliang Zheng, Daqing Liu, Chaoyue Wang, Bing Su, and Changwen Zheng. Sem-MAE: Semantic-guided masking for learning masked autoencoders. 35:14290–14302, 2022a. URL https://proceedings.neurips.cc/paper_files/paper/2022/hash/5c186016d0844767209dc36e9e61441b-Abstract-Conference.html. [Cited on p. 9 and 10.]

Jin Li, Yaoming Wang, Xiaopeng Zhang, Yabo Chen, Dongsheng Jiang, Wenrui Dai, Chenglin Li, Hongkai Xiong, and Qi Tian. Progressively compressed auto-encoder for self-supervised representation learning. 2022b. URL https://openreview.net/forum?id=8T4qmZbTkW7. [Cited on p. 10.]

Zhaowen Li, Zhiyang Chen, Fan Yang, Wei Li, Yousong Zhu, Chaoyang Zhao, Rui Deng, Liwei Wu, Rui Zhao, Ming Tang, and Jinqiao Wang. MST: Masked self-supervised transformer for visual representation, 2021. URL http://arxiv.org/abs/2106.05656. [Cited on p. 2, 9, and 10.]

Xiao Liu, Fanjin Zhang, Zhenyu Hou, Li Mian, Zhaoyu Wang, Jing Zhang, and Jie Tang. Self-supervised learning: Generative or contrastive. *IEEE transactions on knowledge and data engineering*, 35(1):857–876, 2021. URL https://arxiv.org/pdf/2006.08218. [Cited on p. 9.]

Neelu Madan, Nicolae-Cătălin Ristea, Kamal Nasrollahi, Thomas B. Moeslund, and Radu Tudor Ionescu. CL-MAE: Curriculum-learned masked autoencoders. pp. 2492–2502, 2024. URL https://openaccess.thecvf.com/content/WACV2024/html/Madan_CL-MAE_Curriculum-Learned_Masked_Autoencoders_WACV_2024_paper.html. [Cited on p. 9.]

Maxime Oquab, Timothée Darcet, Théo Moutakanni, Huy Vo, Marc Szafraniec, Vasil Khalidov, Pierre Fernandez, Daniel Haziza, Francisco Massa, Alaaeldin El-Nouby, et al. Dinov2: Learning robust visual features without supervision. *arXiv preprint arXiv:2304.07193*, 2023. URL https://arxiv.org/pdf/2304.07193. [Cited on p. 9 and 10.]

Deepak Pathak, Philipp Krahenbuhl, Jeff Donahue, Trevor Darrell, and Alexei A Efros. Context encoders: Feature learning by inpainting. In *Proceedings of the IEEE conference on computer vision and pattern recognition*, pp. 2536–2544, 2016. URL https://arxiv.org/pdf/1604.07379. [Cited on p. 1, 3, and 9.]

Karl Pearson. Liii. on lines and planes of closest fit to systems of points in space. *The London, Edinburgh, and Dublin Philosophical Magazine and Journal of Science*, 2(11):559–572, 1901. doi: 10.1080/14786440109462720. URL https://doi.org/10.1080/14786440109462720. [Cited on p. 3, 10, and 15.]

Aditya Ramesh, Mikhail Pavlov, Gabriel Goh, Scott Gray, Chelsea Voss, Alec Radford, Mark Chen, and Ilya Sutskever. Zero-shot text-to-image generation. In *International conference on machine learning*, pp. 8821–8831. Pmlr, 2021. URL http://proceedings.mlr.press/v139/ramesh21a/ramesh21a.pdf. [Cited on p. 9.]

Bernhard Schölkopf, Alexander Smola, and Klaus-Robert Müller. Kernel principal component analysis. In *International conference on artificial neural networks*, pp. 583–588. Springer, 1997. URL https://link.springer.com/chapter/10.1007/BFb0020217. [Cited on p. 10 and 19.]

Yuge Shi, N. Siddharth, Philip Torr, and Adam R. Kosiorek. Adversarial masking for self-supervised learning. In *Proceedings of the 39th International Conference on Machine Learning*, pp. 20026–20040. PMLR, 2022. URL https://proceedings.mlr.press/v162/shi22d.html. ISSN: 2640-3498. [Cited on p. 2 and 9.]

Matthew Turk and Alex Pentland. Eigenfaces for Recognition. *Journal of Cognitive Neuroscience*, 3(1):71–86, 01 1991. ISSN 0898-929X. doi: 10.1162/jocn.1991.3.1.71. URL https://doi.org/10.1162/jocn.1991.3.1.71. [Cited on p. 9.]

Haochen Wang, Kaiyou Song, Junsong Fan, Yuxi Wang, Jin Xie, and Zhaoxiang Zhang. Hard patches mining for masked image modeling. pp. 10375–10385, 2023. URL https://openaccess.thecvf.com/content/CVPR2023/html/Wang_Hard_Patches_Mining_for_Masked_Image_Modeling_CVPR_2023_paper.html. [Cited on p. 9.]

Zhenda Xie, Zheng Zhang, Yue Cao, Yutong Lin, Jianmin Bao, Zhuliang Yao, Qi Dai, and Han Hu. Simmim: A simple framework for masked image modeling. In *Proceedings of the IEEE/CVF conference on computer vision and pattern recognition*, pp. 9653–9663, 2022. URL https://openaccess.thecvf.com/content/CVPR2022/papers/Xie_SimMIM_A_Simple_Framework_for_Masked_Image_Modeling_CVPR_2022_paper.pdf. [Cited on p. 1 and 9.]

Jiancheng Yang, Rui Shi, Donglai Wei, Zequan Liu, Lin Zhao, Bilian Ke, Hanspeter Pfister, and Bingbing Ni. Medmnist v2-a large-scale lightweight benchmark for 2d and 3d biomedical image classification. *Scientific Data*, 10(1):41, 2023. URL https://www.nature.com/articles/s41597-022-01721-8. [Cited on p. 3, 7, and 15.]

Xiaoyu Yue, Lei Bai, Meng Wei, Jiangmiao Pang, Xihui Liu, Luping Zhou, and Wanli Ouyang. Understanding masked autoencoders from a local contrastive perspective, 2023. URL http://arxiv.org/abs/2310.01994. [Cited on p. 1.]

Qi Zhang, Yifei Wang, and Yisen Wang. How mask matters: Towards theoretical understandings of masked autoencoders. 35:27127–27139, 2022. URL https://proceedings.neurips.cc/paper_files/paper/2022/hash/adb2075b6dd31cb18dfa727240d2887e-Abstract-Conference.html. [Cited on p. 1 and 4.]

Jinghao Zhou, Chen Wei, Huiyu Wang, Wei Shen, Cihang Xie, Alan Yuille, and Tao Kong. ibot: Image bert pre-training with online tokenizer. *arXiv preprint arXiv:2111.07832*, 2021. URL https://arxiv.org/pdf/2111.07832. [Cited on p. 1, 3, and 9.]

A APPENDIX

A.1 PRINCIPAL COMPONENT ANALYSIS

Principal Component Analysis (PCA; Pearson, 1901; Hotelling, 1933) finds a set of orthonormal vectors ($\mathbf{V}$) that maximize the variance of the data. Projecting data samples $\mathbf{X}$ onto $\mathbf{V}$ effectively rotates the original data such that each new variable captures the maximum possible variance while remaining orthogonal to the previous dimensions. When the original data is a linear combination of independent factors (referred to as sources), PCA *can* but does not necessarily recover these sources. PCA recovers mutually statistically independent sources if and only if the original data is jointly Gaussian, since uncorrelatedness implies independence only for the Gaussian distribution. This situation arises, e.g., when the data is a linear combination of Gaussian sources. For data originating from the non-linear combination of sources, PCA *cannot* identify sources thereby leading to statistically dependant principal components.

In this work, we incorporate PCA into the framework of Masked Image Modeling (MIM). Specifically, we propose a task that involves reconstructing masked principal components using the visible ones. This task is meaningful only if it is feasible to approximate the masked PCs based on the visible ones, which occurs when the masked and visible PCs are statistically dependent with one another.

A.2 EXPERIMENTAL SETUP

A.2.1 DATASETS

CIFAR-10 is a widely used benchmark dataset containing 50,000 training and 10,000 validation $32 \times x32$ RGB images depicting 10 object classes, such as airplanes, cars, and animals.

TinyImageNet is a subset of the ImageNet dataset, containing 200 classes of 64×64 RGB images. It consists of 100,000 training images and 10,000 validation images, making it a challenging benchmark for classification tasks with more fine-grained object categories compared to CIFAR-10.

The MedMNIST (Yang et al., 2023) datasets are a collection of medical imaging datasets, each focusing on different types of biomedical data. In this work, three MedMNIST datasets are used:

BloodMNIST consists of 12,000 training and 1,700 validation 64×64 RGB images across 8 classes and represents microscopic images of blood cells, used for hematology classification tasks.

DermaMNIST contains 7,000 training and 1,000 validation 64×64 RGB images of skin samples, each part of one out of 7 types of skin diseases.

PathMNIST comprises 90,000 training and 10,000 validation 64×64 RGB images across 9 classes and depicts histopathological images of colorectal cancer tissue, aiding in classification tasks relevant to pathology.

We apply an equivalent data augmentation strategy to all datasets and for all learning objectives during training; Following He et al. (2021), our augmentation strategy consists of a random cropping followed by image resizing using bicubic interpolation. The scale of the random cropping is fixed to $[0.2, 1.0]$. We add horizontal flipping and we normalize images using each dataset's training mean and standard deviation; We keep these data augmentations during training for evaluation. We find that the use of data augmentations during the evaluation leads to a substantial performance drop for PMAE but we do keep these augmentations for fair comparisons. For all datasets and methods, we define image patches as patches of 8×8 pixels.

A.3 MODEL ARCHITECTURE

We train a tiny Vision Transformer encoder architecture (ViT-T) with image patch size 8×8 for all datasets (ViT-T/8). The specifics of this architecture can be found in Tab. 2. Note that while for MAE, we keep the normalized pixel values of each masked patch as reconstruction targets as

presented in (He et al., 2021), we find it to not have a clear positive impact for PMAE and hence enforce the reconstruction of the raw target values for PMAE.

config	value
hidden size	192
number of attention heads	12
intermediate size	768
norm pixel loss	Y/N
patch size	8×8

Table 2: ViT-T/8 hyperparameters.

config	value
batch size	512
base learning rate	0.00015
optimizer	AdamW [39]
betas (AdamW)	$\beta_1, \beta_2 = 0.9, 0.95$
weight decay	0.05
learning rate (warmup)	0.0003
warmup steps	40

Table 3: Training hyperparameters.

A.4 TRAINING HYPERPARAMETERS

We train the ViT-T encoder-decoder architecture for 800 epochs with the hyperparameters found in Tab. 3. These hyperparameters are taken from (He et al., 2021). We use the linear lr scaling rule: lr = base lr×batchsize / 256 (Goyal, 2017). Note that for our oracle masking setting, we conduct an ablation study across a masking ratio range of $[10, 90]$.

config	value
batch size	512
base learning rate	0.1
optimizer	SGD [6]
betas (SGD)	0.9
learning rate	0.2
warmup steps	10
weight decay	0

Table 4: Linear probing hyperparameters.

config	value
batch size	512
base learning rate	0.001
optimizer	AdamW [39]
betas (AdamW)	$\beta_1, \beta_2 = 0.9, 0.99$
learning rate	0.002
warmup steps	5
weight decay	0.5

Table 5: Fine-tuning hyperparameters.

A.5 EVALUATION HYPERPARAMETERS

We evaluate the learned representation (i.e., [CLS] token) using a linear probe, multi-layer perceptron classifier, and k-Nearest Neighbors algorithm on top of the frozen representation. The training samples of each dataset are used for training and the validation samples for testing. For linear and MLP probing experiments, we train the probes for 100 epochs following common practices (He et al., 2021). For the k-NN algorithm, we tune the number of neighbors in the range $[2, 20]$. More details regarding the linear probing evaluation hyperparameters can be found in Tab. 4. The same hyperparameters were used for the MLP probing. We use the linear lr scaling rule: lr = base lr×batchsize / 256 (Goyal, 2017). For the fine-tuning setup, we also follow (He et al., 2021), finr-tune the encoder and a linear probe for 100 epochs and resort to using the hyperparameters presented in Tab. 5. Note that for PMAE, we evaluate the approach on raw images and do not perform any filtering of principal components prior to evaluation.

A.6 COMPUTATIONAL RESOURCES

All training runs were conducted on a single NVIDIA GeForce RTX 3090/NVIDIA GeForce RTX 4090/Quadro RTX 6000 GPUs or NVIDIA TITAN RTX each of which has 24GB of RAM. Fig. 8

reports the time taken for 800 training epochs using a ViT-T/8 architecture on a Quadro RTX 6000 GPU for CIFAR10 and TinyImageNet with the standard MAE and the PMAE methods.
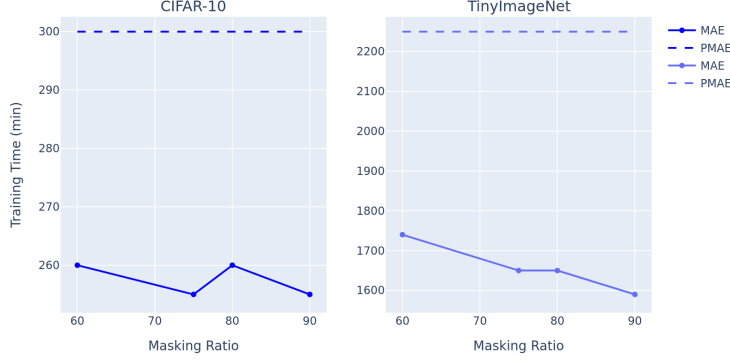

Figure 8: **Training time.** We report the training time in minutes for 800 training epochs using a ViT-T/8 architecture. For standard MAE we report numbers for various masking ratios.

A.7   ADDITIONAL RESULTS

A.7.1   TRAINING DYNAMICS

Fig. 9 displays the linear probe accuracy for varying training epoch checkpoints. Similar to Fig. 9b we observe that PMAE after 100 epochs outperforms MAE after 800 epochs.

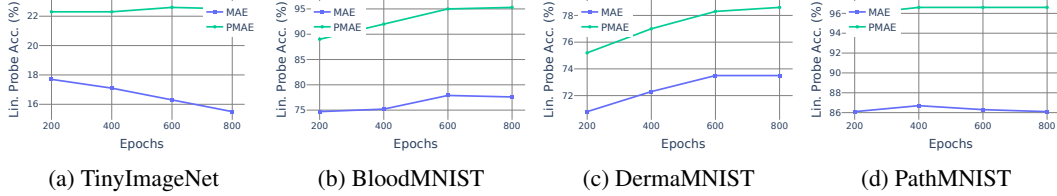(a) TinyImageNet   (b) BloodMNIST   (c) DermaMNIST   (d) PathMNIST

Figure 9: **Performance Curves.** Linear probe accuracy (%) for TinyImageNet, and MedMNIST datasets across training epochs. PMAE, after 200 epochs, outperforms MAE after 800 epochs.

A.7.2 k-NEAREST NEIGHBOR EVALUATION

Tab. 6 shows the classification accuracy for CIFAR10, TinyImageNet, and MedMNIST datasets using a k-NN classifier in place of a linear or MLP probe as presented in Section 5 and Appx. A.7.3.

Table 6: **Evaluation with k-NN.** k-Nearest Neighbors top-1% accuracy for CIFAR10, TinyImageNet and MedMNIST for masking in pixel (MAE) and principal component (PMAE) space with the standard 75% masking ratio (std), oracles (ocl) and randomized (rd) masking ratios. $\star$ and $\star\star$ refer to representations trained with Eq. (3.1) and Eq. (A.1) respectively.

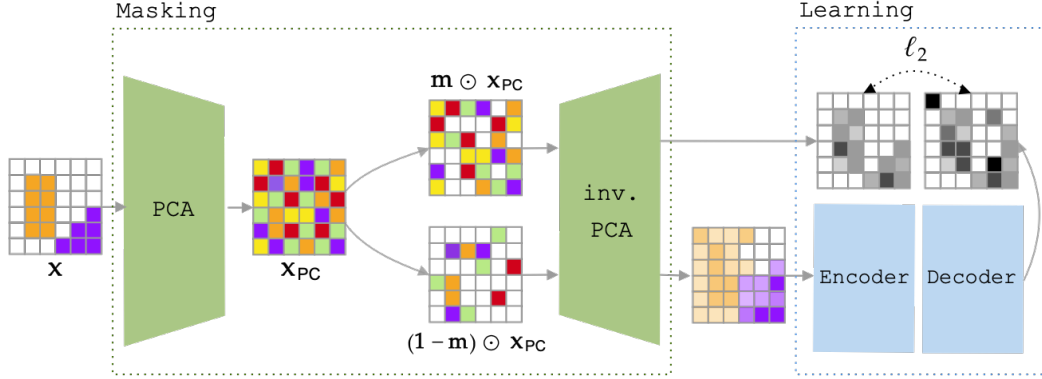|		CIFAR10	TinyImageNet	DermaMNIST	BloodMNIST	PathMNIST
	MAE_{std}	38.3	10.0	71.1	65.7	92.1
	MAE_{ocl}	47.6	12.5	69.9	73.6	94.6
k-**NN**	$\text{PMAE}^{\star}_{\text{ocl}}$	**55.3**	**14.2**	**76.6**	**93.1**	**99.6**
	$\text{PMAE}^{\star\star}_{\text{ocl}}$	48.1	9.6	74.7	84.5	99.1
	MAE_{rd}	40.3	7.6	71.6	82.7	**96.0**
	$\text{PMAE}^{\star}_{\text{rd}}$	41.8	**11.2**	**72.1**	**83.6**	95.5
	$\text{PMAE}^{\star\star}_{\text{rd}}$	**49.6**	9.5	70.6	76.0	94.8

Figure 10: **Overview of the Principal Masked Autoencoder (PMAE) with reconstruction targets in the observation space.** A Principal Masked Autoencoder (PMAE) differs from a vanilla MAE by performing the masking in the space of principal components $\mathbf{x}_{PC} = PCA(\mathbf{x})$ rather than in the observation space. The masked principal component representations $\mathbf{m} \odot \mathbf{x}_{PC}$ and $(\mathbf{1} - \mathbf{m}) \odot \mathbf{x}_{PC}$ are then projected back into the observation space and serve as the reconstruction target and input for an encoder-decoder architecture, respectively.

A.7.3 RECONSTRUCTING IN PIXEL VS. PRINCIPAL COMPONENT SPACE

We further investigate the impact of the domain (i.e., pixel vs. pc space) in which the reconstruction error is minimized on downstream performance. In Fig. 10, we present an alternative to Fig. 1 in which the training objective receives a set of pixels in place of principal components. In Fig. 10, the masked out principal components are projected back into pixel space and the decoder's output is kept as is. The training objective then minimizes the Euclidean distance between the ground truth masked principal components projected back to pixel space and the decoder's output. Instead in Fig. 1 and Eq. (3.1), the training objective minimizes the Euclidean distance between the ground truth and the predicted masked principal components. The learning objective then becomes Eq. (3.1), a modified version of Eq. (A.1):

$$\mathcal{L}_{\text{PMAE}}(\mathbf{x}, \mathbf{m}; \boldsymbol{\theta}, \boldsymbol{\phi}) = \left\| g_{\boldsymbol{\theta}}\left(f_{\boldsymbol{\phi}}\left(t^{-1}\left(\mathbf{m} \odot t\left(\mathbf{x}\right)\right)\right)\right) - t^{-1}\left((\mathbf{1} - \mathbf{m}) \odot t(\mathbf{x})\right) \right\|_2^2, \tag{A.1}$$

Tab. 7 presents the downstream image classification performance achieved when training representations with Eq. (A.1). In particular, it reports results obtained using a linear and MLP probe in the standard, oracle and randomized settings. Despite lower performance gains as the ones presented with Eq. (3.1) in Tab. 1, PMAE consistently outperforms MAE across all five datasets, demonstrating substantial improvements. In Tab. 1 we report an average performance gain of 9.6 percentage points across datasets over the MAE baseline, while Tab. 7 reports an average performance gain of 6.6 percentage points. These findings also support our claims that the space of principal components constitutes a meaningful masking space for Masking Image Modelling learning paradigms.

A.7.4 MASKING RATIO ABLATION

In Appx. A.7.4, we perform an ablation across the masking ratio for representations learned with Eq. (A.1). We draw similar conclusions to the ones drawn from Appx. A.7.4: the optimal masking ratio across datasets lies between 10 and 20% of the variance masked. Above these ratios, we observe a performance drop across datasets. Appx. A.7.4 also shows the impact of the use of data augmentations during training of the linear probe on the downstream accuracy. We see a significant increase in performance for PMAE when dropping data augmentations for the training of the linear probe but still resort to keeping these augmentations for the main results presented in Tab. 1 to ensure a fair comparison with the MAE.

Table 7: Linear & MLP probe and fine-tuning top-1% accuracy for CIFAR10, TinyImageNet and MedMNIST datasets for random masking in pixel (MAE) and principal component (PMAE) space with reconstruction target in pixel space with the standard 75% masking ratio (std), oracles (ocl) and randomized masking ratios (rd). Representations are learnt from Eq. (A.1). * refers to ours.

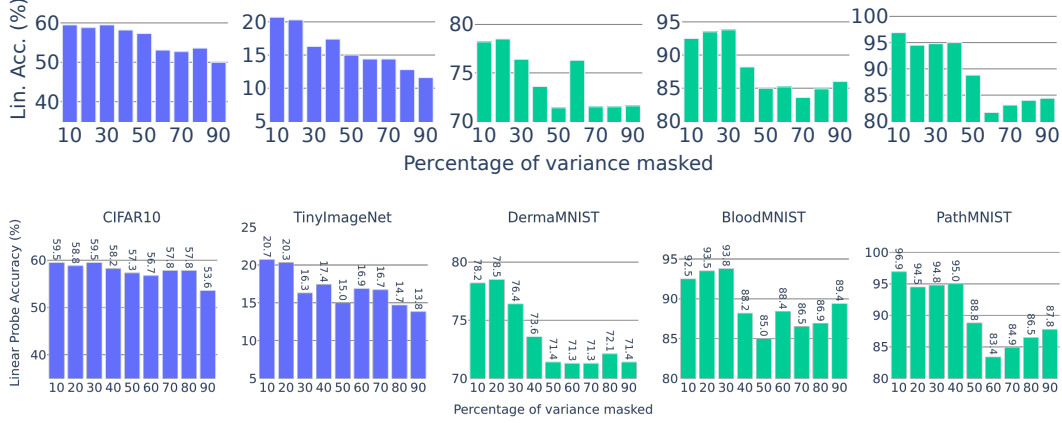|		CIFAR10	TinyImageNet	DermaMNIST	BloodMNIST	PathMNIST
Linear	MAE_{std}	41.7	11.5	72.4	73.4	83.4
	MAE_{ocl}	50.7	15.5	73.7	78.6	86.4
	PMAE^*_{ocl}	**55.1**	**17.4**	**77.4**	**91.0**	**97.0**
	MAE_{rd}	41.9	7.5	72.4	83.2	85.6
	PMAE^*_{rd}	**56.0**	**15.1**	**74.5**	**85.9**	**87.5**
MLP	MAE_{std}	34.0	15.5	72.2	68.6	92.6
	MAE_{ocl}	55.2	**22.2**	74.4	75.8	95.1
	PMAE^*_{ocl}	**61.5**	22.1	**79.6**	**91.0**	**98.8**
	MAE_{rd}	38.5	11.6	66.9	70.6	95.7
	PMAE^*_{rd}	**62.2**	**19.5**	**75.3**	**84.4**	**97.0**

Figure 11: **Impact of the Masking Ratio.** *(top)* PMAE trained with Eq. (A.1) linear probing accuracy for varying masking ratios. We observe a close-to-optimal performance across datasets for 10 to 20% of the variance masked. *(bottom)* PMAE trained with Eq. (A.1) linear probing accuracy *without* data augmentations at evaluation. We observe a significant performance improvement without data augmentations.

A.7.5 BEYOND PCA

Our work shows evidence the PCA offers a meaningful masking space. In Section 6, we motivate our choice by observing that principal components capture global rather than local features of an image. In this section, we go beyond PCA and explore non-linear matrix factorization methods as a proof of concept for future research. In particular, we explore Kernel PCA (Schölkopf et al., 1997) with a Radial Basis Function (RBF) kernel with the kernel coefficient set to 3.10^{-4}. In kernel PCA, the spectral decomposition is performed not on the data itself but rather on a modified version of it: the standardized data is mapped to a high-dimensional space via a non-linear kernel function.

In Tab. 8, we present results on the CIFAR10 dataset and show the image classification accuracy using a linear and MLP probe. We compare a vanilla MAE with our PMAE and KMAE which relies on Kernel PCA for optimal masking ratios (30% of the variance is masked out). For KMAE, we use the setting presented in Appx. A.7.3 and use Eq. (3.1) as the training objective.

The results reveal a significant performance improvement when employing a non-linear image transformation. KMAE achieves an average gain of 13.3 and 5 percentage points compared to the stan-

dard Masked Autoencoder (He et al., 2021) and PMAE, respectively. Although these findings are preliminary and based on a single mid-scale dataset, they highlight the potential of non-linear transformations and further emphasize the value of spectral decomposition as a meaningful for Masked Image Modeling paradigms.

Table 8: Linear and MLP probe top-1% accuracy for CIFAR10 for random masking in pixel (MAE), in principal component space (PMAE) and in Kernel PCA space (KMAE) with the standard 75% masking ratio (std) and oracles (ocl). * refers to ours.

	$\textbf{MAE}_{\text{std}}$	$\textbf{MAE}_{\text{ocl}}$	$\textbf{PMAE}^*_{\text{ocl}}$	$\textbf{KMAE}^*_{\text{ocl}}$
Linear	41.7	50.7	59.0	**64.1**
MLP	34.0	55.2	64.1	**68.6**